**Penn Libraries**
UNIVERSITY OF PENNSYLVANIA

University of Pennsylvania
**ScholarlyCommons**

Departmental Papers (MSE)

Department of Materials Science & Engineering

December 2007

# Distortion of 3D SU8 Photonic Structures Fabricated by Four-beam Holographic Lithography with Umbrella Configuration

Xuelian Zhu
*University of Pennsylvania*

Shu Yang
*University of Pennsylvania*, shuyang@seas.upenn.edu

Yongan Xu
*University of Pennsylvania*

Follow this and additional works at: http://repository.upenn.edu/mse_papers

# Distortion of 3D SU8 Photonic Structures Fabricated by Four-beam Holographic Lithography with Umbrella Configuration

**Abstract**

We present a quantitative study of the distortion from a three-term diamond-like structure fabricated in SU8 polymer by four-beam holographic lithography. In the study of the refraction effect, theory suggests that the lattice in SU8 should be elongated in the [111] direction but have no distortion in the (111) plane, and each triangular-like hole array in the (111) plane would rotate by ~30º away from that in air. Our experiments agree with the prediction on the periodicity in the (111) plane and the rotation due to refraction effect, however, we find that the film shrinkage during lithographic process has nearly compensated the predicted elongation in the [111] direction. In study of photonic bandgap (PBG) properties of silicon photonic crystals templated by the SU8 structure, we find that the distortion has decreased quality of PBG.

**Comments**

Reprinted from *Optics Express*, Volume 15 Issue 25, December 2007, pages 16546-16560.

# Distortion of 3D SU8 Photonic Structures Fabricated by Four-beam Holographic Lithography with Umbrella Configuration

**Xuelian Zhu, Yongan Xu, and Shu Yang***

*Department of Materials Science & Engineering, University of Pennsylvania,*
*3231 Walnut Street, Philadelphia, PA 19104*
*shuyang@seas.upenn.edu*

**Abstract:** We present a quantitative study of the distortion from a three-term diamond-like structure fabricated in SU8 polymer by four-beam holographic lithography. In the study of the refraction effect, theory suggests that the lattice in SU8 should be elongated in the [111] direction but have no distortion in the (111) plane, and each triangular-like hole array in the (111) plane would rotate by $\sim 30^{\circ}$ away from that in air. Our experiments agree with the prediction on the periodicity in the (111) plane and the rotation due to refraction effect, however, we find that the film shrinkage during lithographic process has nearly compensated the predicted elongation in the [111] direction. In study of photonic bandgap (PBG) properties of silicon photonic crystals templated by the SU8 structure, we find that the distortion has decreased quality of PBG.

---

### References and links

1. E. Yablonovitch, "Inhibited spontaneous emission in solid-state physics and electronics," Phys. Rev. Lett. **58**, 2059-2062 (1987).
2. John, "Strong localization of photons in certain disordered dielectric superlattices," Phys. Rev. Lett. **58**, 2486-2489 (1987).
3. A. Mekis, J. C. Chen, I. Kurland, S. H. Fan, P. R. Villeneuve, and J. D. Joannopoulos, "High transmission through sharp bends in photonic crystal waveguides," Phys. Rev. Lett. **77**, 3787-3790 (1996).
4. A. Chutinan, and S. Noda, "Highly confined waveguides and waveguide bends in three-dimensional photonic crystal," Appl. Phys. Lett. **75**, 3739-3741 (1999).
5. Y. Akahane, T. Asano, B. S. Song, and S. Noda, "High-Q photonic nanocavity in a two-dimensional photonic crystal," Nature **425**, 944-947 (2003).
6. J. P. Dowling, M. Scalora, M. J. Bloemer, and C. M. Bowden, "The photonic band edge laser: a new approach to gain enhancement," J. Appl. Phys. **75**, 1896-1899 (1994).
7. T. Prasad, V. Colvin, and D. Mittleman, "Superprism phenomenon in three-dimensional macroporous polymer photonic crystals," Phys. Rev. B **67**, 165103 (2003).
8. P. V. Parimi, W. T. T. Lu, P. Vodo, and S. Sridhar, "Photonic crystals - Imaging by flat lens using negative refraction," Nature **426**, 404-404 (2003).
9. S. Y. Lin, J. G. Fleming, D. L. Hetherington, B. K. Smith, R. Biswas, K. M. Ho, M. M. Sigalas, W. Zubrzycki, S. R. Kurtz, and J. Bur, "A three-dimensional photonic crystal operating at infrared wavelengths," Nature **394**, 251-253 (1998).
10. M. Campbell, D. N. Sharp, M. T. Harrison, R. G. Denning, and A. J. Turberfield, "Fabrication of photonic crystals for the visible spectrum by holographic lithography," Nature **404**, 53-56 (2000).
11. Y. A. Vlasov, X. Z. Bo, J. C. Sturm, and D. J. Norris, "On-chip natural assembly of silicon photonic bandgap crystals," Nature **414**, 289-293 (2001).
12. A. C. Edrington, A. M. Urbas, P. DeRege, C. X. Chen, T. M. Swager, N. Hadjichristidis, M. Xenidou, L. J. Fetters, J. D. Joannopoulos, Y. Fink, and E. L. Thomas, "Polymer-based photonic crystals," Adv. Mater. **13**, 421-425 (2001).
13. S. R. Kennedy, M. J. Brett, O. Toader, and S. John, "Fabrication of tetragonal square spiral photonic crystals," Nano Lett. **2**, 59-62 (2002).

14. G. M. Gratson, M. Xu, and J. A. Lewis, "Microperiodic structures - Direct writing of three-dimensional webs" Nature **428**, 386 (2004).
15. K. K. Seet, V. Mizeikis, S. Matsuo, S. Juodkazis, and H. Misawa, "Three-dimensional spiral-architecture photonic crystals obtained by direct laser writing," Adv. Mater. **17**, 541-545 (2005).
16. J. H. Moon, J. Ford, and S. Yang, "Fabricating three-dimensional polymer photonic structures by multi-beam interference lithography," Polym. Adv. Technol. **17**, 83–93 (2006).
17. M. Thiel, M. Decker, M. Deubel, M. Wegener, S. Linden, and G. von Freymann, "Polarization stop bands in chiral polymeric three-dimensional photonic crystals," Adv. Mater. **19**, 207-210 (2007).
18. W. Haske, V. W. Chen, J. M. Hales, W. T. Dong, S. Barlow, S. R. Marder, and J. W. Perry, "65 nm feature sizes using visible wavelength 3-D multiphoton lithography," Opt. Express **15**, 3426-3436 (2007).
19. S. R. Marder, J. L. Bredas, and J. W. Perry, "Materials for multiphoton 3D microfabrication," MRS Bull. **32**, 561-565 (2007).
20. Y. V. Miklyaev, D. C. Meisel, A. Blanco, G. von Freymann, K. Busch, W. Koch, C. Enkrich, M. Deubel, and M. Wegener, "Three-dimensional face-centered-cubic photonic crystal templates by laser holography: fabrication, optical characterization, and band-structure calculations," Appl. Phys. Lett. **82**, 1284-1286 (2003).
21. Y. K. Lin, and P. R. Herman, "Effect of structural variation on the photonic band gap in woodpile photonic crystal with body-centered-cubic symmetry," J. Appl. Phys. **98**, 063104 (2005).
22. R. L. Sutherland, V. P. Tondiglia, L. V. Natarajan, S. Chandra, D. Tomlin, and T. J. Bunning, "Switchable orthorhombic F photonic crystals formed by holographic polymerization-induced phase separation of liquid crystal," Opt. Express **10**, 1074-1082 (2002).
23. C. K. Ullal, M. Maldovan, E. L. Thomas, G. Chen, Y. J. Han, and S. Yang, "Photonic crystals through holographic lithography: Simple cubic, diamond-like, and gyroid-like structures," Appl. Phys. Lett. **84**, 5434-5436 (2004).
24. Y. C. Zhong, S. A. Zhu, H. M. Su, H. Z. Wang, J. M. Chen, Z. H. Zeng, and Y. L. Chen, "Photonic crystal with diamondlike structure fabricated by holographic lithography," Appl. Phys. Lett. **87**, 061103 (2005).
25. D. C. Meisel, M. Diem, M. Deubel, F. Perez-Willard, S. Linden, D. Gerthsen, K. Busch, and M. Wegener, "Shrinkage precompensation of holographic three-dimensional photonic-crystal templates," Adv. Mater. **18**, 2964-2968 (2006).
26. Y. Lin, P. R. Herman, and K. Darmawikarta, "Design and holographic fabrication of tetragonal and cubic photonic crystals with phase mask: toward the mass-production of three-dimensional photonic crystals," Appl. Phys. Lett. **86**, 071117 (2005).
27. Y. Lin, D. Rivera, and K. P. Chen, "Woodpile-type photonic crystals with orthorhombic or tetragonal symmetry formed through phase mask techniques," Opt. Express **14**, 887-892 (2006).
28. W. D. Mao, J. W. Dong, Y. C. Zhong, G. Q. Liang, and H. Z. Wang, "Formation principles of two-dimensional compound photonic lattices by one-step holographic lithography," Opt. Express **13**, 2994-2999 (2005).
29. J. Xu, R. Ma, X. Wang, and W. Y. Tam, "Icosahedral quasicrystals for visible wavelengths by optical interference holography," Opt. Express **15**, 4287-4295 (2007).
30. C. K. Ullal, M. Maldovan, M. Wohlgemuth, E. L. Thomas, C. A. White, and S. Yang, "Triply periodic bicontinuous structures through interference lithography: a level-set approach," J. Opt. Soc. Am. A **20**, 948-954 (2003).
31. H. Lorenz, M. Despont, N. Fahrni, N. LaBianca, P. Renaud, and P. Vettiger, "SU-8: a low-cost negative resist for MEMS," J. Micromech. Microeng. **7**, 121-124 (1997).
32. M. Born and E. Wolf, *Principles of Optics: Electromagnetic Theory of Propagation, Interference and Diffraction of Light* (Cambridge University Press, Cambridge, U.K.; New York, 1999).
33. J. H. Moon, S. Yang, W. T. Dong, J. W. Perry, A. Adibi, and S. M. Yang, "Core-shell diamond-like silicon photonic crystals from 3D polymer templates created by holographic lithography," Opt. Express **14**, 6297-6302 (2006).
34. L. Z. Cai, X. L. Yang, and Y. R. Wang, "All fourteen Bravais lattices can be formed by interference of four noncoplanar beams," Opt. Lett. **27**, 900-902 (2002).
35. D. C. Meisel, M. Wegener, and K. Busch, "Three-dimensional photonic crystals by holographic lithography using the umbrella configuration: Symmetries and complete photonic band gaps," Phys. Rev. B **70**, 165104 (2004).
36. *International Tables for Crystallography. Vol A, Space-Group Symmetry* (Kluwer, Dordrecht, London, 2002).
37. *International Tables for Crystallography. Vol. B, Reciprocal Space* (Kluwer, Dordrecht, Boston, 2001).
38. W. H. Zhou, S. M. Kuebler, K. L. Braun, T. Y. Yu, J. K. Cammack, C. K. Ober, J. W. Perry, and S. R. Marder, "An efficient two-photon-generated photoacid applied to positive-tone 3D microfabrication," Science **296**, 1106-1109 (2002).
39. S. Yang, M. Megens, J. Aizenberg, P. Wiltzius, P. M. Chaikin, and W. B. Russel, "Creating periodic three-dimensional structures by multibeam interference of visible laser," Chem. Mater. **14**, 2831-2833 (2002).
40. S. Jeon, J.-U. Park, R. Cirelli, S. Yang, C. E. Heitzman, P. V. Braun, P. J. A. Kenis, and J. A. Rogers, "Fabricating complex three-dimensional nanostructures with high-resolution conformable phase masks," Proc. Nat. Acad. Sci. USA **101**, 12428-12433 (2004).

41. T. Kondo, S. Juodkazis, and H. Misawa, "Reduction of capillary force for high-aspect ratio nanofabrication," Appl. Phys. A **81**, 1583-1586 (2005).
42. S. G. Johnson, and J. D. Joannopoulos, "Block-iterative frequency-domain methods for Maxwell's equations in a planewave basis," Opt. Express **8**, 173-190 (2001).
43. J. S. King, E. Graugnard, O. M. Roche, D. N. Sharp, J. Scrimgeour, R. G. Denning, A. J. Turberfield, and C. J. Summers, "Infiltration and inversion of holographically defined polymer photonic crystal templates by atomic layer deposition," Adv. Mater. **18**, 1561-1565. (2006).
44. J. H. Moon, Y. Xu, Y. Dan, S. M. Yang, A. T. Johnson, and S. Yang, "Triply periodic bicontinuous structures as templates for photonic crystals: A pinch-off problem," Adv. Mater. **19**, 1510-1514 (2007).
45. T. Y. M. Chan, O. Toader, and S. John, "Photonic band gap templating using optical interference lithography," Phys. Rev. E **71**, 046605 (2005).
46. T. Y. M. Chan, O. Toader, and S. John, "Photonic band-gap formation by optical-phase-mask lithography," Phys. Rev. E **73**, 046610 (2006).

## 1. Introduction

Photonic crystals (PCs)[1, 2] with periodic dielectric microstructures are of interest for numerous applications in optical integrated circuits, including micro-wave scale, single-mode waveguides with sharp bends[3, 4], high-Q resonant cavities[5], distributed feedback lasers[6], superprisms[7], and perfect lenses[8]. To realize three-dimensional (3D) photonic crystals with complete photonic bandgaps (PBGs), various methods have been studied to fabricate high-quality 3D photonic structures [9-19]. Among them, holographic lithography (HL) holds promise as an efficient and flexible technique for creating a wide range of defect-free 3D microstructures, including face-centered cubic (f.c.c)[20], body-center-cubic (b.c.c)[21], orthorhombic F[22], diamond-like[23, 24], simple cubic[25], gyroid-like structures[23], woodpile-type[26, 27], compound lattices[28], as well as quasicrystals[29] by controlling the beam geometry, polarization, phase, and intensity in HL. During exposure, the multiple-beam interference intensity profile is transferred to a thick photoresist film, followed by post-exposure bake and development to create the microporous structures. The shape of the resulting structure is determined by the isodose surface of the lithographic threshold value, which can be described by the corresponding level surface[30]. In the level-set approach, the surface of a porous dielectric structure is represented by a scalar-valued function $F$, which satisfies $F(x, y, z)=t$, where $t$ is a constant to control the volume fraction.

While many 3D photonic structures with large complete bandgaps have been proposed theoretically, in HL experiments most of the structures are fabricated from a thick negative-tone photoresist, SU8, which has an average of eight epoxy groups per chain. Since SU8 has a refractive index of ~ 1.6, the influence of refraction at the air/film interface cannot be ignored when the beams travel from the air (n=1) into the resist film. To avoid this problem, many workers have applied prisms and/or index matching liquids[20, 23, 25] to precompensate the effects of refraction. However, little has been studied quantitatively beyond the intuition of how the structure can be distorted by the refraction effect. The availability of specific prisms and index-matching liquids for many of the structures and polymer systems could further hamper the broader application of HL for fabrication of a wider range of 3D photonic structures. In addition, it is not uncommon to expect shrinkage of the photoresists during photoexposure and development, especially in the case of negative-tone resists, which could further distort the fabricated structures. Therefore, theoretical analysis can impart great benefits on the rationale design of 3D photonic structures by revealing the underlying mechanisms of structural distortion during each processing step and their impact to photonic bandgap properties. On the basis of the knowledge, we could later exploit novel designs of photoresist systems and optical setups to experimentally realize crystals with large complete bandgaps. To this end, we reconstructed the unit cells and level surfaces of the 3D structures in SU8 vs. those in air by considering refraction and film shrinkage separately.

SU8 is an ultrathick photoresist that has been widely used in microelectromechanical systems (MEMS)[31] and HL[10, 20, 23] to fabricate high aspect ratio microstructures and PCs. Therefore, it was chosen as the model photoresist to study here. Using the three-term

diamond-like lattice as a target, we compared the reconstructed structures predicted by theory with that fabricated experimentally using four-beam HL in an umbrella configuration (see Table 1 for optical system parameters) to elucidate the origin of structure distortion. When considering refraction only, the calculation suggested lattice stretching along the [111] direction in SU8 film, resulting in change of translational symmetry from f.c.c. (in air) to rhombohedral (in SU8), and a rotation of the triangular-like hole array in the (111) plane by ~ 30° away from that in air attributed to change of polarization terms. While we experimentally confirmed such rotation and almost no change of periodicity in the (111) plane as predicted, no elongation in the [111] direction was observed, which might be due to anisotropic shrinkage of SU8 film along the [111] direction during lithographic processing. Overall, the symmetry of the fabricated SU8 structure was decreased, with the space group changing from $R\bar{3}m$ (in air) to $R32$ (in SU8). After considering both refraction and shrinkage effects, we reconstructed the level surfaces, which matched well with experimental results. Finally, we investigated the PBGs of inverse 3D Si PCs templated from the SU8 structure. The calculation showed that the structure distortion would decrease the quality factors of PBGs.

## 2. Theoretic Analysis

The analysis was conducted step-by-step as illustrated in Scheme 1.
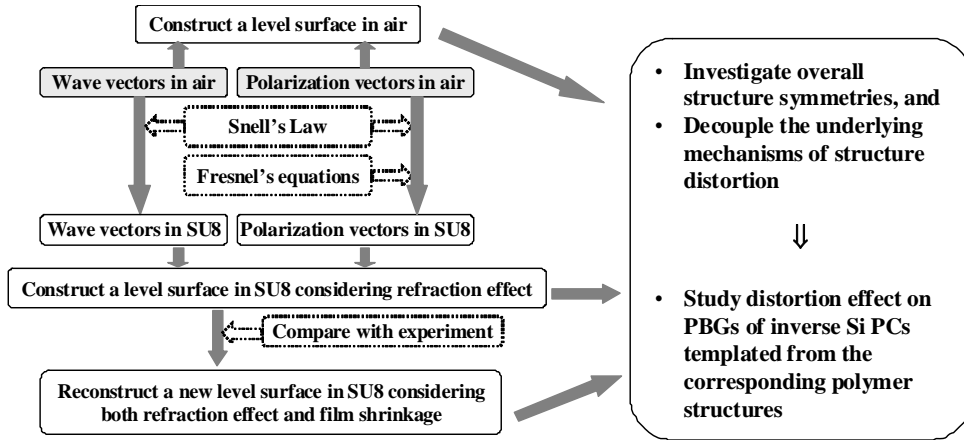


Scheme 1. Flow chart illustrating the step-by-step theoretical analysis.

### 2.1 Refraction effect on both wave vectors and polarization parameters

We investigate the effect of refraction on wave vectors, which determine the geometry of the reciprocal lattice of the fabricated structure, and polarization vectors, including the direction and the strength of the electric field. As shown in Scheme 2, we first considered an arbitrary light beam with wavelength λ, wave vector $\vec{k} = \frac{2\pi}{\lambda}[l,m,n]$, where $l$, $m$, $n$ are direction cosines, and the polarization represented by the complex electric field vector $\vec{E} = [E_x, E_y, E_z]$. The beam propagates from air into a dielectric medium with refractive index $n_r$, and the normal direction is $\hat{u}_n$. The angle of refraction $\theta'$ is determined by Snell's Law[32], $\sin\theta' = \sin\theta/n_r$, where $\theta$ is the incident angle.

If the incident beam is perpendicular to the interface between the air and the dielectric medium, the new wave vector is equal to $\vec{k}' = \frac{2\pi n_r}{\lambda}[l,m,n]$, along the same direction of the incident beam. For an oblique incident beam, three independent equations are required to determine the new wave vector $\vec{k}' = \frac{2\pi n_r}{\lambda}[l',m',n']$ in the dielectric medium. The first

equation is to define the normalization condition, $\dfrac{\vec{k}'}{\left|\vec{k}'\right|}=1$. The second one is related to the

angle between $\vec{k}'$ and $\hat{u}_n$, $\theta'$, $\dfrac{\vec{k}'}{\left|\vec{k}'\right|}\cdot\hat{u}_n=\cos\theta'=\sqrt{1-(\dfrac{\sin\theta}{n_r})^2}$. Finally, the third constraint is to

confine the three vectors, $\vec{k}$, $\vec{k}'$ and $\hat{u}_n$, to the same plane: $\dfrac{\vec{k}'}{\left|\vec{k}'\right|}\cdot\dfrac{\hat{u}_n\times\vec{k}}{\left|\vec{k}\right|}=0$.
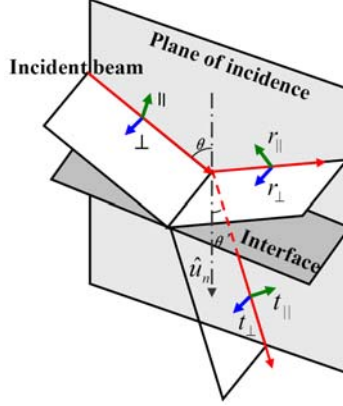


Scheme 2. Schematic illustration of light propagation from air to the dielectric medium.

Likewise, we need to calculate the new polarization vectors in the dielectric medium. The transmission coefficients from air to a non-magnetic dielectric medium are described by Fresnel's equations[32]:

$$t_\perp=\left(\frac{E'}{E}\right)_\perp=\frac{2\cos\theta}{\cos\theta'+n_r\cos\theta} \qquad (1)$$

$$t_\parallel=\left(\frac{E'}{E}\right)_\parallel=\frac{2\cos\theta}{\cos\theta+n_r\cos\theta'} \qquad (2)$$

where, the subscript $\perp$ denotes the polarization with the electric field perpendicular to the plane of incidence (shown in blue in scheme 2), and $\parallel$ for the parallel one (shown in green in Scheme 2).

If the incident beam is perpendicular to the interface between the air and the dielectric medium, $t_\perp=t_\parallel\hat{=}t$, and the new polarization is described as $\vec{E}'=t[E_x,\ E_y,\ E_z]$. If the incident beam is oblique, the electric field vector $\vec{E}$ of the incident beam has to be separated into two components: one is perpendicular ( $E_\perp=\vec{E}\cdot\dfrac{\hat{u}_n\times\vec{k}}{\left|\vec{k}\right|\mathrm{Sin}(\theta)}$ ) and the other is parallel

( $E_\parallel=\vec{E}\cdot\dfrac{\hat{u}_n\times\vec{k}\times\vec{k}}{\left|\vec{k}\right|^2\mathrm{Sin}(\theta)}$ ) to the incident plane. Applying Fresnel's Eq. (1) and (2), the components

of the electric field in the dielectric medium can then be calculated as $\vec{E}'_\perp=t_\perp E_\perp\dfrac{\hat{u}_n\times\vec{k}'}{\left|\vec{k}'\right|\sin\theta'}$ and

$\vec{E}'_\parallel=t_\parallel E_\parallel\dfrac{\hat{u}_n\times\vec{k}'\times\vec{k}'}{\left|\vec{k}'\right|^2\sin\theta'}$, respectively. Therefore, the new polarization vector is obtained as

$$\vec{E}' = \vec{E}'_\perp + \vec{E}'_\parallel = [E'_x, E'_y, E'_z] \tag{3}$$
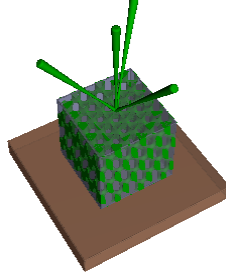


Scheme 3. Schematic illustration of the four-beam HL in the umbrella configuration.

With both wave vectors and polarization parameters for an arbitrary single beam defined in the dielectric medium, we investigated the effects of refraction on interference intensity profile of four-beam HL in an umbrella configuration (Scheme 3). In our experiment, the laser source (diode-pumped Nd:YVO$_4$ laser from Coherent, wavelength $\lambda = 532$ nm) was split into four beams, where the central beam was right-circularly polarized and perpendicular to the surface of the photoresist SU8 (n ~1.6 at $\lambda = 532$ nm), and the other three were linearly polarized and oblique at 39$^o$ relative to the central one. The circular polarization of the central beam distributes equal intensity to the surrounding beams and has been widely used in the fabrication of 3D PCs by HL[24, 33]. The intensity ratio between the central beam and the side beams was 2:1:1:1. It is noted that no prism or index matching liquid was used in our optical setup, thus, the incident beams reached the surface of SU8 film directly. The original parameters in air and the calculated new wave vectors and polarization vectors in the SU8 for the four-beam umbrella HL are summarized in Table 1.

Table 1. Wave vectors and polarization vectors in air and SU8 using interference lithography with visible light ($\lambda = 532$ nm).

| Medium | Air | SU8 |
|---|---|---|
| Refractive index | 1.0 | 1.6 |
| Wave vectors | $\vec{k}_0 = \dfrac{2\pi}{\lambda}[\dfrac{1}{\sqrt{3}}, \dfrac{1}{\sqrt{3}}, \dfrac{1}{\sqrt{3}}];$ $\vec{k}_1 = \dfrac{2\pi}{\lambda}[\dfrac{5}{3\sqrt{3}}, \dfrac{1}{3\sqrt{3}}, \dfrac{1}{3\sqrt{3}}];$ $\vec{k}_2 = \dfrac{2\pi}{\lambda}[\dfrac{1}{3\sqrt{3}}, \dfrac{5}{3\sqrt{3}}, \dfrac{1}{3\sqrt{3}}];$ $\vec{k}_3 = \dfrac{2\pi}{\lambda}[\dfrac{1}{3\sqrt{3}}, \dfrac{1}{3\sqrt{3}}, \dfrac{5}{3\sqrt{3}}].$ | $\vec{k}'_0 = \dfrac{2\pi * 1.6}{\lambda}[\dfrac{1}{\sqrt{3}}, \dfrac{1}{\sqrt{3}}, \dfrac{1}{\sqrt{3}}];$ $\vec{k}'_1 = \dfrac{2\pi * 1.6}{\lambda}[0.852, 0.371, 0.371];$ $\vec{k}'_2 = \dfrac{2\pi * 1.6}{\lambda}[0.371, 0.852, 0.371];$ $\vec{k}'_3 = \dfrac{2\pi * 1.6}{\lambda}[0.371, 0.371, 0.852].$ |
| Polarization vectors | $\vec{E}_0 = \sqrt{2}$ [circular polarization]; $\vec{E}_1 = \pm[-0.25, 0.345, 0.905];$ $\vec{E}_2 = \pm[0.905, -0.25, 0.345];$ $\vec{E}_3 = \pm[0.345, 0.905, -0.25].$ | $\vec{E}'_0 = 1.088$ [circular polarization]; $\vec{E}'_1 = \pm 0.715 [-0.484, 0.286, 0.827];$ $\vec{E}'_2 = \pm 0.715 [0.827, -0.484, 0.286];$ $\vec{E}'_3 = \pm 0.715 [0.286, 0.827, -0.484].$ |

## 2.2 Interference intensity profiles in air and polymer film

The stationary intensity profile created by the interference of multiple coherent beams is given by

$$I(\vec{r}) = \sum_{l=0}^{N-1} \sum_{m=0}^{N-1} \vec{E}_l \cdot \vec{E}_m^* \exp[i(\vec{k}_l - \vec{k}_m) \cdot \vec{r}] \tag{4}$$

For *N*=4, Eq. (4) is rewritten as

$$I(\vec{r}) = I_0 + 2 \sum_{\substack{l,m=0 \\ l<m}}^{3} \{\text{Re}(\vec{E}_l \cdot \vec{E}_m^*) \cos[(\vec{k}_l - \vec{k}_m) \cdot \vec{r}] - \text{Im}(\vec{E}_l \cdot \vec{E}_m^*) \sin[(\vec{k}_l - \vec{k}_m) \cdot \vec{r}]\} \tag{5}$$

where $I_0 = \sum_{l=0}^{3} |E_l|^2$ .

Since the circular polarization has no preferred direction, it can be projected in two arbitrary perpendicular directions in the plane normal to the wave vector $\vec{k}_0$, which is denoted as the *A* plane.

$$\vec{E}_0 = \frac{E_0}{\sqrt{2}} \hat{a} \pm i \frac{E_0}{\sqrt{2}} \hat{b} \tag{6}$$

where, $\hat{a}$ and $\hat{b}$ are two perpendicular directions in the *A* plane, and the + and − signs represent right- and left-handed rotation, respectively.

To determine the coefficients $\vec{E}_0 \cdot \vec{E}_j^*$ (*j*=1, 2, 3), the polarization vector $\vec{E}_j$ is projected on the *A* plane:

$$\vec{E}_j^{\,inA} = \vec{E}_j - (\vec{E}_j \cdot \frac{\vec{k}_0}{|\vec{k}_0|}) \frac{\vec{k}_0}{|\vec{k}_0|} \tag{7}$$

Assuming the angle between $\vec{E}_j^{\,inA}$ and the $\hat{a}$ axis is $\theta_j$,

$$\vec{E}_0 \cdot \vec{E}_j^* = \frac{E_0}{\sqrt{2}} |\vec{E}_j^{\,inA}| (\cos[\theta_j] \pm i \sin[\theta_j]) \tag{8}$$

and

$$\begin{aligned} &\text{Re}(\vec{E}_0 \cdot \vec{E}_j^*) \cos[(\vec{k}_0 - \vec{k}_j) \cdot \vec{r}] - \text{Im}(\vec{E}_0 \cdot \vec{E}_j^*) \sin[(\vec{k}_0 - \vec{k}_j) \cdot \vec{r}] \\ &= \frac{E_0}{\sqrt{2}} |\vec{E}_j^{\,inA}| \cos[(\vec{k}_0 - \vec{k}_j) \cdot \vec{r} \pm \theta_j] \end{aligned} \tag{9}$$

Given the angle between the $\vec{E}_i^{\,inA}$ and $\vec{E}_j^{\,inA}$ as $\alpha_{ij}$ (from $\vec{E}_i^{\,inA}$ to $\vec{E}_j^{\,inA}$, anticlockwise is positive, clockwise is negative, and $\alpha_{ii}=0$), we would have $\alpha_{ij}=\theta_j - \theta_i$ (*i*, *j* = 1, 2, 3).

Since the three surrounding beams were linearly polarized in our optical setup, $\vec{E}_j = \vec{E}_j^*$ (*j*=1, 2, 3), and Eq. (5) can be rewritten as

$$I(\vec{r}) = I_0 + 2 \{ \sum_{i=1}^{3} \frac{E_0}{\sqrt{2}} |\vec{E}_i^{\,inA}| \cos[(\vec{k}_0 - \vec{k}_i) \cdot \vec{r} \pm \theta_i] + \sum_{\substack{i,j=1 \\ i<j}}^{3} (\vec{E}_i \cdot \vec{E}_j) \cos[(\vec{k}_i - \vec{k}_j) \cdot \vec{r}] \} \tag{10}$$

In Eq. (10), the phase factor $\theta_j$ ($j$=1, 2, 3) can be simultaneously eliminated by a translation of the origin by $\vec{\rho} = \sum_{j=1}^{3} \theta_j \vec{\eta}_j$ , where $\vec{\eta}_j$ satisfies $(\vec{k}_0 - \vec{k}_i) \cdot \vec{\eta}_j = \mp \delta_{ij}$ , where $\delta_{ij}$ =1 for $i$=$j$, and $\delta_{ij}$ =0 for $i \neq j$. After this shift, the intensity profile in Eq. (10) can be rewritten as $I(\vec{r} + \vec{\rho})$ , in which the phase terms are

$$(\vec{k}_0 - \vec{k}_i) \cdot (\vec{r} + \vec{\rho}) \pm \theta_i = (\vec{k}_0 - \vec{k}_i) \cdot (\vec{r} + \sum_{j=1}^{3} \theta_j \vec{\eta}_j) \pm \theta_i = (\vec{k}_0 - \vec{k}_i) \cdot \vec{r} \mp \theta_i \pm \theta_i = (\vec{k}_0 - \vec{k}_i) \cdot \vec{r} \quad (11)$$

$$(\vec{k}_i - \vec{k}_j) \cdot (\vec{r} + \vec{\rho}) = (\vec{k}_i - \vec{k}_j) \cdot \vec{r} + [(\vec{k}_0 - \vec{k}_j) - (\vec{k}_0 - \vec{k}_i)] \cdot \sum_{s=1}^{3} \theta_s \vec{\eta}_s = (\vec{k}_i - \vec{k}_j) \cdot \vec{r} \mp \alpha_{ij} \quad (12)$$

and the intensity profile $I(\vec{r} + \vec{\rho})$ is simplified to

$$I(\vec{r}) = I_0 + 2 * \{ \sum_{i=1}^{3} \frac{E_0}{\sqrt{2}} \left| \vec{E}_i^{\,in\,A} \right| \cos[(\vec{k}_0 - \vec{k}_i) \cdot \vec{r}] + \sum_{\substack{i,j=1 \\ i<j}}^{3} (\vec{E}_i \cdot \vec{E}_j) \cos[(\vec{k}_i - \vec{k}_j) \cdot \vec{r} \mp \alpha_{ij}] \} \quad (13)$$

where the – (or +) sign is for the optical system with a right- (or left-) circularly polarized central beam, and $I_{left}(\vec{r}) = I_{right}(-\vec{r})$ . From Eq. (13), it is clear that the intensity profiles are independent of the phase factor $\theta_j$ induced by the circular polarization.

It is important to note that the intensity profile does not change by the signs of $\pm \vec{E}_j$ ($j$=1, 2, 3), which are indistinguishable in the experiment. According to Eq. (13), the first four terms remain the same no matter whether we reverse any one, two or all three directions of $\vec{E}_j$. In the last three terms, however, when the sign of $\vec{E}_i \cdot \vec{E}_j$ changes, the $\alpha_{ij}$ would have a phase shift of $\pm \pi$ , that is $-(\vec{E}_i \cdot \vec{E}_j) \cos[(\vec{k}_i - \vec{k}_j) \cdot \vec{r} \mp (\alpha_{ij} \pm \pi)] = (\vec{E}_i \cdot \vec{E}_j) \cos[(\vec{k}_i - \vec{k}_j) \cdot \vec{r} \mp \alpha_{ij}]$ . Hence, Eq. (13) would be identical for any combination of the polarization vectors $\pm \vec{E}_j$.
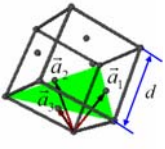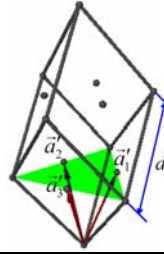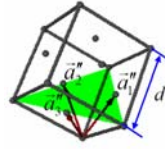
## 3. Results and discussion

### 3.1 Effect of refraction on lattice parameters and level surfaces: theoretical analysis

From the beam parameters in air and SU8 (Table 1), we calculated the corresponding reciprocal and real lattices based on the method described in reference [34] (see Table 2 for respective lattice parameters). The interference pattern in air was designed to have f.c.c. translational symmetry. However, after considering the influence of refraction, the lattice was stretched along the [111] direction and became rhombohedral in SU8. For the simplicity of comparing the two lattices, we kept the four lattice points in the rhombohedral unit cell the same as those in f.c.c. The lattice constants are $d$ = 1.38 μm for the f.c.c, and $d'$ = 1.78 μm for the rhombohedral lattice, respectively. The two lattices were plotted to scale and the corresponding lattice parameters are summarized in Table 2. In the plots, the red arrows represent the basis vectors of the primary lattices, which have length of 0.98 μm for f.c.c and 1.49 μm for rhombohedral lattice, respectively. It is known the angle between the lattices basis vectors of f.c.c is 60°. Due to refraction, this angle changes to 38.3° in SU8 because of the elongation in [111] direction. To quantify the difference between the two lattices, we compared the changes in the (111) plane and [111] direction. The (111) planes are shown as green triangles. We found that the distance between the nearest neighbors remained the same for both lattices (0.98 μm), indicating that there was no lattice distortion in the (111) plane. However, due to refraction from air to SU8, the distance between the adjacent lattice planes in

the [111] direction increased from 0.80 μm (f.c.c in air) to 1.38 μm (rhombohedra in SU8). At the same time the shape of the pattern changes. More discussion will be given later in the text.

Table 2. Lattice parameters for the interference patterns in air and in SU8. ($c = 2\pi/d$ and $d = 1.38$μm.)

| Medium | Air | SU8 (considering refraction effect only) | SU8 (considering both refraction and film shrinkage) |
|---|---|---|---|
| Reciprocal lattice vectors | $\vec{b}_1 = c[-1,1,1];$ $\vec{b}_2 = c[1,-1,1];$ $\vec{b}_3 = c[1,1,-1].$ | $\vec{b}_1' = c[-1.140, 0.860, 0.860];$ $\vec{b}_2' = c[0.860, -1.140, 0.860];$ $\vec{b}_3' = c[0.860, 0.860, -1.140];$ | $\vec{b}_1'' = c[-1.006, 0.994, 0.994];$ $\vec{b}_2'' = c[0.994, -1.006, 0.994];$ $\vec{b}_3'' = c[0.994, 0.994, -1.006];$ |
| Real lattice vectors | $\vec{a}_1 = 0.5d[0,1,1];$ $\vec{a}_2 = 0.5d[1,0,1];$ $\vec{a}_3 = 0.5d[1,1,0].$ | $\vec{a}_1' = 0.743d\ [0.327, 1, 1];$ $\vec{a}_2' = 0.743d\ [1, 0.327, 1];$ $\vec{a}_3' = 0.743d\ [1, 1, 0.327];$ | $\vec{a}_1'' = 0.506d\ [0.013, 1, 1];$ $\vec{a}_2'' = 0.506d\ [1, 0.013, 1];$ $\vec{a}_3'' = 0.506d\ [1, 1, 0.013];$ |
| Plot of real lattices |  |  |  |
| Translational symmetry | Fcc | Rhombohedral | Rhombohedral |
| Lattice constant $d$ (μm) | 1.38 | 1.78 | 1.39 |
| $\left| \vec{a}_j \right|$ (μm) | 0.98 | 1.49 | 0.99 |
| Angle between $\vec{a}_i$ & $\vec{a}_j$ | 60º | 38.3º | 59.1º |
| Distance between the nearest lattice points in (111) plane (μm) | 0.98 | 0.98 | 0.98 |
| Distance between the adjacent lattice planes in [111] direction $h_{111}$ (μm) | 0.80 | 1.38 | 0.81 |
| Space groups of the corresponding level surfaces | No. 166 ( $R\bar{3}m$ ) | No.155 ($R32$) | No.155 ($R32$) |

The change of lattice parameters due to refraction in turn alters the level surface that describes the structure symmetry. Given the central beam is right-circularly polarized, the level surfaces in air and in SU8 were derived from the interference intensity profile [Eq. (13)] as the following:

$$F_{\text{air}}(\vec{r}) = \cos[\frac{2\pi}{d}(-x+y+z)] + \cos[\frac{2\pi}{d}(x-y+z)] + \cos[\frac{2\pi}{d}(x+y-z)] \qquad (14)$$

and

$$F_{\text{SU8}}(\vec{r}) = \cos[\frac{2\pi}{d}(-1.140x + 0.860y + 0.860z)] + \cos[\frac{2\pi}{d}(0.860x - 1.140y + 0.860z)]$$
$$+ \cos[\frac{2\pi}{d}(0.860x + 0.860y - 1.140z)] + 0.301\ \cos[\frac{2\pi}{d} \cdot 2(x-y) - \frac{\pi}{3}]$$
$$+ 0.301\ \cos[\frac{2\pi}{d} \cdot 2(y-z) - \frac{\pi}{3}] + 0.301\ \cos[\frac{2\pi}{d} \cdot 2(z-x) - \frac{\pi}{3}]$$

$$(15)$$

where $d = 3\sqrt{3}\lambda / 2 = 1.38$ μm. The structure is defined as

$$F(\vec{r}) > t \text{ for dielectric, and } F(\vec{r}) < t \text{ for air} \qquad (16)$$

where $t$ is a constant to control the filling volume fraction. In the case that the central beam is left-circularly polarized, the level surfaces comply with $F_{\text{left}}(\vec{r}) = F_{\text{right}}(-\vec{r})$ since $I_{\text{left}}(\vec{r}) = I_{\text{right}}(-\vec{r})$ according to Eq. (13). Here, only the right-circular polarization is discussed.

The symmetries of the interference patterns in air and SU8 could be investigated from the corresponding level surfaces. Eq. (14) describes a three-term diamond-like structure in air, which belongs to space group No.166 ( $R\bar{3}m$ ) [35] with inversed symmetry, that is $F_{\text{air}}(-\vec{r}) = F_{\text{air}}(\vec{r})$. For the symmetry of the level surface in SU8 as described by Eq. (15), we applied the method used in reference [35] assuming $x_r = -1.140x + 0.860y + 0.860z$, $y_r = 0.860x-1.140y+0.860z$, and $z_r = 0.860x+0.860y-1.140z$. Eq. (15) can be simplified as

$$F_{\text{SU8}}(\vec{r}_r) = \cos(\frac{2\pi}{d}x_r) + \cos(\frac{2\pi}{d}y_r) + \cos(\frac{2\pi}{d}z_r)$$
$$+ v\{\cos[\frac{2\pi}{d}(x_r - y_r)] + \cos[\frac{2\pi}{d}(y_r - z_r)] + \cos[\frac{2\pi}{d}(z_r - x_r)]\}$$
$$- q\{\sin[\frac{2\pi}{d}(x_r - y_r)] + \sin[\frac{2\pi}{d}(y_r - z_r)] + \sin[\frac{2\pi}{d}(z_r - x_r)]\}$$
$$\propto \tilde{A}_{100}^{No.155} + v\ \tilde{A}_{1\bar{1}0}^{No.155} - q\ \tilde{B}_{1\bar{1}0}^{No.155}$$

$$(17)$$

where $v = 0.301\cos(\pi/3)$, $q = 0.301\sin(\pi/3)$,

$$\tilde{A}_{hkl}^{No.155} = [\cos(hx_r + ky_r + lz_r) + \cos(lx_r + hy_r + kz_r) + \cos(kx_r + ly_r + hz_r)]$$
$$+ [\cos(kx_r + hy_r + lz_r) + \cos(lx_r + ky_r + hz_r) + \cos(hx_r + ly_r + kz_r)]$$

and

$$\tilde{B}_{hkl}^{No.155} = [\sin(hx_r + ky_r + lz_r) + \sin(lx_r + hy_r + kz_r) + \sin(kx_r + ly_r + hz_r)]$$
$$- [\sin(kx_r + hy_r + lz_r) + \sin(lx_r + ky_r + hz_r) + \sin(hx_r + ly_r + kz_r)]$$

The geometric structure factor $F_{hkl}^{No.155}$, which is invariant under the symmetry operations of the corresponding space group, can be written as $F_{hkl}^{No.155} = \tilde{A}_{hkl}^{No.155} + i\tilde{B}_{hkl}^{No.155}$ [36, 37].

Therefore, the structure of the interference pattern in SU8 is consistent with No.155 ($R32$), which has no inversion symmetry, that is, $F_{\mathrm{SU8}}(-\vec{r}) \neq F_{\mathrm{SU8}}(\vec{r})$ .
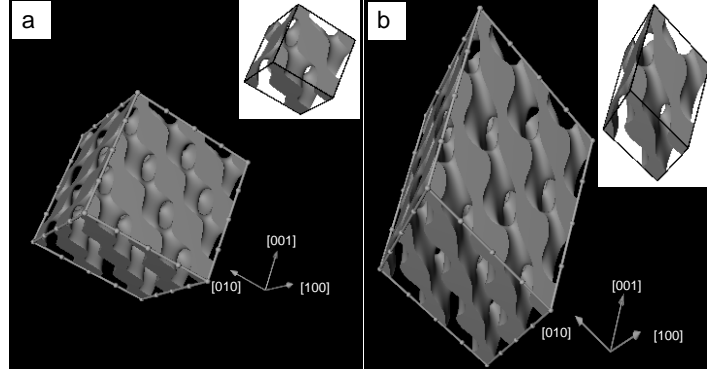


Fig. 1. Level surfaces of (a) three-term diamond-like structure in air described by Eq. (14), $t_{\mathrm{air}}$=0, the filling fraction of dielectric materials is 50%, and (b) distorted SU8 structure described by Eq. (15), $t_{\mathrm{SU8}}$=0, the filling fraction of SU8 is 48%. All surfaces belong to the {100} family planes. The unit length on the 3D frame of (a) is $d/2$, where the lattice constant, $d$ =1.38 μm, and that of (b) is $d'/2$, and $d'$ =1.78 μm. Insets: corresponding unit cells.

The structures in air and in SU8 are plotted in Fig. 1, assuming $t_{\mathrm{air}} = t_{\mathrm{SU8}} = 0$, corresponding to a filling fraction of 50% and 48%, respectively. Each pattern consists of eight unit cells (see Fig. 1 insets), and all the top surfaces belong to the {100} family planes. The level surface from SU8 shown in Fig. 1 (b) clearly illustrates the elongation in the [111] direction by the influence of refraction compared with that in air [Fig. 1 (a)].
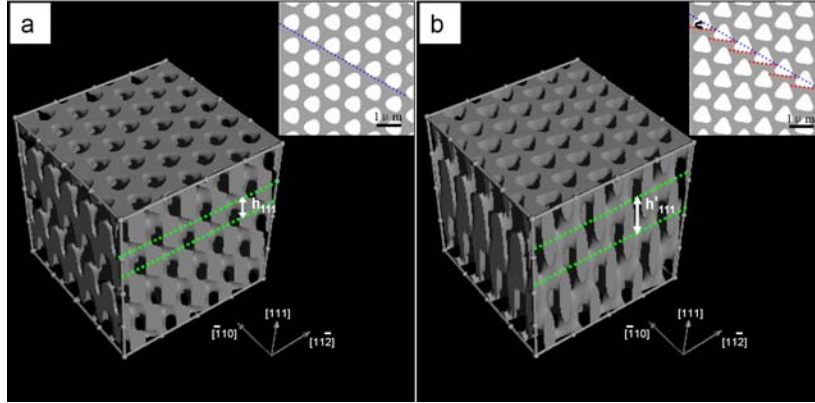


Fig. 2. Level surfaces of (a) three-term diamond-like structure in air with filling fraction of the dielectric materials as 50% [Eq. (14), $t_{\mathrm{air}}$=0], and (b) distorted SU8 structure with the filling fraction of SU8 as 48% [Eq. (15), $t_{\mathrm{SU8}}$=0]. In both images, the top surface is the (111) plane, the left side is the (11$\bar{2}$) plane, and the right side is the ($\bar{1}$10) plane. The unit length in the 3D frames: $d$ = 1.38 μm. Insets: 2D cut of the top surfaces.

To quantitatively analyze the change of the resulting interference structures in the (111) plane and the [111] direction, we cut the level surfaces in the (111), ($\bar{1}$10) and (11$\bar{2}$) planes, which are perpendicular to each other as shown in Fig. 2. The elongation in the [111] direction is clear from the ($\bar{1}$10) and (11$\bar{2}$) planes: the distance between the adjacent lattice planes in the [111] direction is $h_{111}$=0.80 μm in air and $h'_{111}$=1.38 μm in the distorted SU8 structure. Similar to the discussion in lattice parameters, the distance between the holes in the (111) plane remained the same, 0.98 μm, for both structures in air and in SU8. However, the

triangular-like hole array in the (111) plane was found rotated ~30° in the distorted SU8 structure since the motifs of the two structures were different. Our calculation suggested that the rotation was caused by the interference terms between the three oblique surrounding beams, which disappeared in the air since the three polarization vectors of the side beams were pairwise perpendicular to each other.

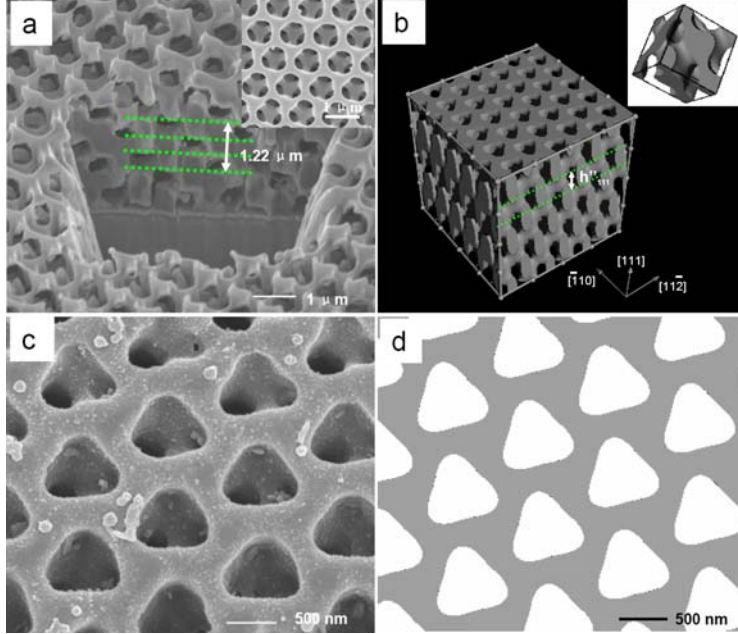*3.2 Comparison between theoretical values and experimental results*



Fig. 3. (a) Close-up SEM image of the fabricated SU8 structure with the top surface tilted by 30°. The cross-section is FIB milled perpendicular to the (111) plane. The green dotted lines indicate four adjacent (111) lattice planes. Taking into account the viewing angle (60°), the distance between the adjacent lattice planes in the [111] direction is $h_{111}$=0.81 μm. The top (111) plane is partially melted by the ion beam. Inset: the (111) plane before FIB milling. (b) Distorted SU8 structure described by Eq. (18) with a filling fraction of 48% ($t'_{SU8}$=0) by considering both refraction and film shrinkage. The top surface is the (111) plane, the left one is the ($11\bar{2}$) plane, and the right one is the ($\bar{1}10$) plane. The unit length of the frame is $d$ = 1.38 μm. Inset: the unit cell. (c) The bottom layer of the SU8 structure. (d) 2D cut of the (111) plane from Fig. 3(b).

To validate the theoretical prediction and investigate the contributions of refraction and possible film shrinkage to the structure distortion, we fabricated 3D SU8 structures following the procedure reported previously[33] (see parameters in Table 1, with the central beam right-circularly polarized). To prevent pattern collapse of the 3D porous film during air drying, we dried the film using supercritical $CO_2$ dryer (SAMDRI®-PVT-3D from tousimis) after the development. As seen in Fig. 3(a), the top surface (111) plane tilted by 30° in the fabricated SU8 structure as predicted. From the SEM images, we measured the distance between the holes in the (111) plane as ~ 0.97 μm, which was close to the calculated value, 0.98 μm. The lattice period in the [111] direction was measured as ~ 0.81 μm from SEM by milling the film using focused-ion-beam (FIB). The result was much smaller than the calculated 1.38 μm, but nearly identical to that in air, 0.80 μm. The significant difference between experiment and theory may be attributed to the large shrinkage of SU8 during the lithographic process, including photopolymerization and solvent development steps[25]. The shrinkage problem is well-known in the application of negative-tone resists (e.g. epoxy and acrylates)[38]. Upon exposure to light, the low-molecular weight SU8 resin polymerizes and crosslinks into an infinite network based on a cationic ring opening reaction, leading to shrinkage in the film.

The percentage of shrinkage depends on the level of epoxy functionality involved in photocrosslinking, the exposure dosage and post-exposure bake time and temperature. In addition, during development, the organic solvent would swell the crosslinked film, which further distorts the patterned film after drying. We note that the distortion caused by resist shrinkage is different from the pattern collapse caused by capillary force exerted during development, rinsing and drying steps, which is dependent on the wetting contact angle, surface tension of the developer/rinsing solvent, and pattern geometry. For the later, it can be addressed by the use of supercritical drying[39, 40] or the selection of a solvent with a sufficiently large contact angle[41]. However, these methods do not alleviate the film shrinkage, which is dependent on the photoresist chemistry and the film crosslinking density.

If we define the shrinkage as $s_r = (c_{cal} - c_{exp})/c_{cal}$, the shrinkage is ~ 1% in the (111) plane, and ~ 41% in the [111] direction, respectively, which agrees well with the results from a different SU8 structure patterned by HL[25]. Since the bottom layer of SU8 film was confined by the substrate while the perpendicular direction was free, it is not surprising that the 3D structure shrank anisotropically.

Considering both refraction effect and resist shrinkage with respect to the resulting HL polymer structure, we modified Eq. (15) by taking the following steps to construct a new level surface:

Step 1, rotate the [111] direction to any axis of $x$, $y$ or $z$,

Step 2, compressing a specific axis along [111] direction while keeping the other two axes fixed, and

Step 3, rotate everything back to the original coordinates.

For simplicity, we assume that the SU8 film was crosslinked uniformly and shrank uniformly ~ 41% along the [111] direction. Therefore, the new level surface can be constructed as

$$
\begin{aligned}
F'_{SU8}(\vec{r}) = {}& \cos[\frac{2\pi}{d}(-1.006x + 0.994y + 0.994z)] + \cos[\frac{2\pi}{d}(0.994x - 1.006y + 0.994z)] \\
& + \cos[\frac{2\pi}{d}(0.994x + 0.994y - 1.006z)] + 0.301\cos[\frac{2\pi}{d} \cdot 2(x-y) - \frac{\pi}{3}] \\
& + 0.301\cos[\frac{2\pi}{d} \cdot 2(y-z) - \frac{\pi}{3}] + 0.301\cos[\frac{2\pi}{d} \cdot 2(z-x) - \frac{\pi}{3}]
\end{aligned}
\tag{18}
$$

where $d$ = 1.38 μm. Eq. (18) also shows a noninversion symmetric structure and belongs to the space group No.155 ($R32$), which is plotted in Fig. 3(b) with $t'_{SU8}$=0, corresponding to a filling fraction of 48%.

The lattice parameters of the structure given in Eq. (18) are calculated (Table 2). After considering both effects (refraction and film shrinkage), the reconstructed SU8 structure is close to the f.c.c lattice in air except that the triangular-like hole array in the (111) plane rotates by ~30° [Fig. 3 (c) and (d)]. This implies that the resist shrinkage nearly compensates the lattice stretching due to refraction of the wave vectors but not polarization vectors. It is interesting to note that the air holes in the top surface [inset in Fig. 3(a)] appeared more rounded than those in the bottom layer [Fig. 3(c)]. This can again be explained by the film shrinkage. The air holes in the top surface were allowed to expanded to a more circular shape to minimize the surface energy, whereas the bottom layer of the resist film was confined by the substrate, therefore, appeared more triangular as defined by the interference pattern.

*3.3 Influence of structure distortion on photonic bandgap (PBG) properties*

Since polymers typically have low refractive indices, the HL patterned polymer structures are often used as templates for backfilling of high index materials to realize complete PBGs[33]. Here, we chose silicon with a dielectric constant of 13 as the backfilling materials and calculated the PBG properties using the MIT Photonic-Band Package[42] based on the level surfaces described by Eqs. (14), (15) and (18), respectively. We and others have shown that

complete filling of HL patterned bicontinuous structures through top-down approaches, such as CVD process[33] and atomic layer deposition (ALD) [43] are challenging: the pore sizes are not uniform and the narrowest channel pinches off (i.e., disconnect) before reaching the maximum filling fraction due to the formation of a core-shell structure[44]. Alternatively, wet chemistry methods may offer promise to improve the filling fraction[44]. Since the focus of this paper is to study the structure distortion during HL patterning and its impact on PBG properties, here, we assume that the template is completely filled as commonly practiced in the literatures[23, 35, 45, 46].
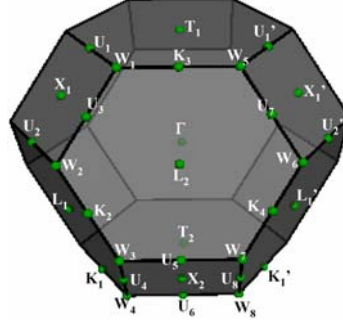


Fig. 4. High-symmetry points of the Brillouin zone of the distorted structure [Eq. (15) and (18)] belonged to space group No.155 ($R32$).

The rhombohedral Brillouin zone (BZ) for the distorted structure [No.155 ($R32$)] is shown in Fig. 4, which has larger irreducible BZ than the three-term diamond-like structure [No.166 ($R\bar{3}m$)] depicted in reference [35]. As seen in Fig. 5(a), the inverse Si PC templated from the non-distorted three-term diamond-like template [Eq. (14)] show two complete PBGs: one between the second and third band with a maximum quality factor (gap/mid-gap ratio) of 5.3% at an optimum filling fraction $f_{si}$=38%, and the other between the seventh and eighth band with a quality factor peak of 3.7% at $f_{si}$=24%. The refraction at air/film intereface leads to lattice stretching along the [111] direction [Eq. (15)], resulting in the loss of complete PBGs. When considering both refraction and film shrinkage, the complete PBGs reappear [Fig. 5(b)]. However, because the symmetry of the level surface in SU8 is lower than that in air, the quality factor peak decreased to 1.5% at a filling fraction of 36% for the PBG between the second and third band, and less than 0.2% for PBG between the seventh and eighth band. Furthermore, the filling fraction range of each PBG shrank, e.g., from $f_{si}$ = 27% - 57% (for three-term diamond-like structure) to 28% - 48% (for the distorted structure) between the second and third band.
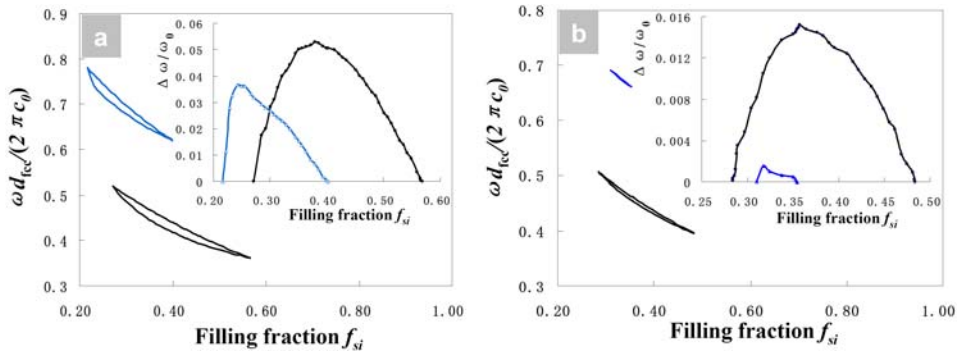


Fig. 5. PBG maps of silicon PCs templated from (a) three-term diamond-like structure [Eq.(14)] and (b) distorted structure by taking into account of both refraction and film shrinkage [Eq.(18)]. Insets: quality factor vs. filling fraction. Black lines: the gap between the second and third band, and blue lines: the gap between the seventh and eighth band. $d_{fcc}$=1.38μm and $c_0$ is the light velocity in vacuum.

14

## 4. Conclusion

We have quantitatively studied the distortion of a three-term diamond-like structure fabricated by four-beam holographic lithography from SU8 resist, which can be attributed to 1) refraction at the air-film interface, and 2) resist film shrinkage during lithographic process. To understand the effect of refraction, we compared the interference intensity profile and reconstructed level surfaces in SU8 (n ~ 1.6) with those in.air (n=1). Our calculation suggested that the SU8 lattice was stretched along the [111] direction but no distortion in the (111) plane in comparison with that in air, and the symmetry of their level surface decreased from space group No.166 ( $R\bar{3}m$ ) in air to No.155 ($R32$) in SU8. Therefore, the translational symmetry was decreased from f.c.c in air to rhombohedral in SU8. It also suggested that the SU8 pattern would rotate by ~ 30$^o$ in the (111) plane away from that in air due to the effects of refraction on polarization. In experiments, we confirmed the rotation of ~ 30$^o$ and almost no change of periodicity in the (111) plane. However, no elongation in the [111] direction was observed, which was attributed to SU8 resist shrinkage during the lithographic process. Because resist shrinkage could not compensate refraction from the polarization vectors, the overall symmetry of the SU8 structure remained low, No.155 ($R32$). By considering both refraction and film shrinkage, we reconstructed the level surface that matched well with experimental results. Finally, using SU8 structures as templates for backfilling, we calculated the PBGs of the inversed distorted 3D Si PCs, and observed decrease of the quality factors. We believe that the presented quantitative understanding of distortion in three-term diamond-like SU8 films can be applied to many other 3D polymer templates patterned by holographic lithography. It offers the first important step toward rationale design of appropriate optical systems and resist systems for desired photonic crystals with large complete bandgaps.